Molecular Therapy
Nucleic Acids
Original Article

Cas9 editing of *ATXN1* in a spinocerebellar ataxia type 1 mice and human iPSC-derived neurons

Kelly J. Fagan,[1,2] Guillem Chillon,[1,3] Ellie M. Carrell,[1] Elisa A. Waxman,[1,5] and Beverly L. Davidson[1,4,5]

[1]Raymond G. Perelman Center for Cellular and Molecular Therapeutics, The Children's Hospital of Philadelphia, Philadelphia, PA, USA; [2]Cell and Molecular Biology Graduate Group, Biomedical Graduate Studies, University of Pennsylvania, Philadelphia, PA, USA; [3]Bioengineering Graduate Program, School of Engineering and Applied Science, University of Pennsylvania, Philadelphia, PA, USA; [4]Department of Pathology & Laboratory Medicine, University of Pennsylvania, Philadelphia, PA, USA; [5]Center for Epilepsy and NeuroDevelopmental Disorders (ENDD), The Children's Hospital of Philadelphia, University of Pennsylvania Perelman School of Medicine, Philadelphia, PA, USA

Spinocerebellar ataxia type 1 (SCA1) is an adult-onset neurodegenerative disease caused by an expansion of the CAG repeat region of the *ATXN1* gene. Currently there are no disease-modifying treatments; however, previous work has shown the potential of gene therapy, specifically RNAi, as a potential modality. Cas9 editing offers potential for these patients but has yet to be evaluated in SCA1 models. To test this, we first characterized the number of transgenes harbored in the common B05 mouse model of SCA1. Despite having five copies of the human mutant transgene, a 20% reduction of *ATXN1* improved behavior deficits without increases in inflammatory markers. Importantly, the editing approach was confirmed in induced pluripotent stem cell (iPSC) neurons derived from patients with SCA1, promoting the translatability of the approach to patients.

INTRODUCTION

Spinocerebellar ataxia type 1 (SCA1) is an adult-onset neurodegenerative disease that causes progressive deterioration of motor coordination and bulbar dysfunction, including speech difficulties. SCA1 is one of many microsatellite disorders and is characterized by a CAG repeat expansion in exon 8 of the *ATXN1* gene.[1–4] The expanded CAG region results in an extended polyglutamine (polyQ) repeat, which confers pathology. In SCA1, the disease phenotype manifests at 39 to more than 100 uninterrupted CAG repeats in this region. *ATXN1* is expressed ubiquitously; however, pathology is primarily evident in cerebellar Purkinje cells (PCs).[5]

The B05 transgenic mouse models SCA1 through the expression of human *ATXN1* (h*ATXN1*), with 82 uninterrupted CAG repeats in PCs.[6,7] This model recapitulates aspects of the human disease, including transcriptional changes, progressive motor dysfunction, and PC degeneration and death. Although expression of *ATXN1* is observed throughout the body in human patients, this model of PC-specific expression has been useful in elucidating the physiological role of *ATXN1* and as a preclinical model for various therapeutics.[8–10] Wild-type (WT) ATXN1 protein functions as a transcriptional repressor and interacts with proteins such as capicua (CIC).[11,12] These interactions are altered in the context of mutant ATXN1 causing transcriptional dysregulation, which is likely a key driver of pathogenicity.[8] Various therapeutic avenues have been explored for SCA1, including supplementation of neurotrophic factor brain-derived neurotrophic factor, restoring ion channel dysfunction, or lithium treatment.[13–15] However, due to the monogenic nature of SCA1, targeting *ATXN1* with gene-silencing therapies may be a potential treatment option.

Currently, there is no cure for SCA1, and treatment consists of symptom management.[16] Recent work has demonstrated the benefit of antisense oligonucleotides (ASOs) and RNAi in preclinical studies targeting h*ATXN1* or mouse *Atxn1* in expansion knockin models.[10,17] ASOs are short, single-stranded nucleic acids that can alter gene expression through splicing, translating, or promoting cleavage via RNaseH.[18] ASOs targeting *ATXN1* were shown to decrease motor deficits in a knockin model of SCA1; however, a limitation of this treatment modality is the requirement for repeated administration to maintain therapeutic benefit, which can be challenging for patients. As a long-term knockdown strategy, recombinant adeno-associated virus (rAAV) has been used to deliver artificial microRNAs (miRNAs) targeting *ATXN1*.[9,19] This strategy can both prevent SCA1 disease onset and reverse disease phenotypes when delivered post-symptom onset. miRNAs rely on endogenous cellular machinery to process pre-miRNAs to the mature miRNA for incorporation into the silencing complex, resulting in RNA knockdown.[20] AAV-based miRNA must be continually expressed to maintain low *ATXN1* transcript levels.

Received 20 January 2024; accepted 29 August 2024;
https://doi.org/10.1016/j.omtn.2024.102317.

Correspondence: Beverly L. Davidson, Raymond G. Perelman Center for Cellular and Molecular Therapeutics, The Children's Hospital of Philadelphia, Philadelphia, PA, USA.
E-mail: davidsonbl@chop.edu

CRISPR-Cas9 gene editing presents another method to induce the reduction of mutant *ATXN1* transcripts. Cas9 scans the genome for complementarity to the guide RNA (gRNA), and upon binding, utilizes the nuclease domain to induce a double-stranded break (DSB).[21,22] Cellular machinery, upon creation of a DSB, will repair the site typically through non-homologous end joining, a fast but error-prone repair pathway that results in the creation of an indel and can lead to nonsense mediated decay (NMD) in resultant transcripts. Cas9 editing has been used preclinically to target repeat expansion diseases.[23–25] For Huntington disease (HD), targeting the expanded Huntington allele with a single gRNA has been shown to rescue pathology in an HD mouse model, and excision of the CTG repeat expansion in myotonic dystrophy using a dual gRNA strategy has been demonstrated in both cell lines and mice.[26,27]

Given the known therapeutic efficacy of reducing *ATXN1* levels, we hypothesized that using CRISPR-Cas9 strategies to target *ATXN1* would be therapeutically beneficial. Here, we test two Cas9-mediated approaches for *ATXN1* reduction and assess the editing outcomes in the B05 mouse model and iPSC-derived neurons. Our data show successful editing in model systems, with Cas9-mediated behavior improvements in SCA1 mice.

RESULTS

Dual and single gRNA strategies edit *ATXN1 in vitro*

CRISPR-Cas9 gRNAs were designed to target *ATXN1* using either a single gRNA or a dual gRNA strategy. The *ATXN1* gene comprises 9 exons, with only exons 8 and 9 included in the coding sequence. We initially screened gRNAs for both strategies in HEK293 cells to assess *ATXN1* knockdown. For the single gRNA strategy, gRNAs were screened near the start codon of exon 8 and upstream of the exon-exon junction (EEJ) (Figure S1A). Targeting the EEJ induced higher levels of RNA knockdown compared to start site gRNAs, with EE2 being the most efficient gRNA (Figures 1A, S1B, and S1D; Table S1).

The dual gRNA strategy flanks the CAG repeat region and was designed to remove the CAG repeat region when both gRNAs cleave simultaneously. For initial screening, three gRNAs targeting upstream of the CAG repeat region (CAG1,2,3) were combined with three gRNAs targeting downstream (CAG4,5,6) (Figures 1A and S1A; Table S1). CAG3+6 resulted in significant *ATXN1* RNA and protein knockdown and was selected for future experiments (Figures S1C and S1D). Subsequently, EE2 and CAG3+6 were cloned into rAAV shuttle plasmids (Figure 1B) and transfected into *Sp*Cas9-expressing HEK293 cells for analysis of DNA and RNA. Both the single and dual gRNAs significantly decrease *ATXN1* RNA 56% and 57% of normal levels, respectively (Figure 1C). ATXN1 protein levels were significantly reduced—39% for single gRNA and 43% for dual gRNA strategies (Figures 1D and S2). To assess indel formation, we designed a droplet digital PCR (ddPCR) drop-off assay for the single gRNA strategy (Figure 1G). Following EGFP sorting for positively transfected cells, analysis of single gRNA-edited sites showed 30% indels in edited samples compared to control transfected cells (Figure 1H). For the dual gRNA strategy, the deletion was confirmed by sequencing of amplified regions (Figures 1E and 1F). These data show that single and dual gRNA strategies target *ATXN1* to significantly reduce endogenous human *ATXN1* mRNA levels *in vitro*.

Analysis of B05 mouse model and *in vivo* editing of *ATXN1*

The efficacy of gRNAs was assessed *in vivo* using the well-characterized B05 mouse model. One limitation, however, is the reported 25–30 copies of the human mutant allele, composed of *ATXN1* cDNA, integrated into the genome.[6] Thus, this model has the potential to dilute gRNA efficiency because of the many optimal binding sites, which differs from normal, with two sites per genome. To reconfirm transgene copy number calculated earlier using Southern blots,[6] ddPCR analysis of genomic DNA of the B05 mouse was done. These data show five copies per diploid genome (Figure 2A). Next, mRNA levels of various transcripts within the cerebella of B05 and WT mice were measured to assess changes with disease progression at 4 weeks (pre-symptomatic in B05 mice), 26 weeks (symptomatic), and 50 weeks (late disease). PC protein 2 (*Pcp2*) showed a 30% and 50% reduction at 26 and 50 weeks, respectively, depicting the progressive cerebellar degeneration observed in SCA1 mice (Figure 2B). Interestingly, h*ATXN1* levels, driven from the Pcp2 promoter, did not mirror endogenous *Pcp2* levels. h*ATXN1* mRNA levels increased from 4 to 26 weeks and remained unchanged to 50 weeks (Figure 2C). We also assessed calbindin (*Calb*) levels and endogenous mouse *Atxn1* levels in B05 and WT mice. *Calb* levels decreased to 40% normal levels by 26 weeks and then remained unchanged at 50 weeks (Figure S3A). There were no differences in mouse *Atxn1* levels across ages in diseased or WT mice, and no changes with age in *Pcp2* or *Calb* in WT mice (Figures S3B–S3E). *ATXN1* levels were also assessed in a recently described knockin model of SCA1 to better understand the nature of the h*ATXN1* upregulation in B05 cerebella with age.[28] Q146 mice have one copy of the coding region of endogenous mouse *Atxn1* replaced with the h*ATXN1* coding region with 146 CAG repeats.[28] In Q146 mice, cerebellar h*ATXN1* and *Pcp2* levels decreased significantly from 8 to 30 weeks of age (Figures S4A and S4B). There were no changes in h*ATXN1* levels over time in striata in Q146 mice, consistent with the lack of degeneration seen in this model (Figure S4A).[28] These data indicate that the increased levels of h*ATXN1* observed in aged B05 animals are intrinsic to the model and not reflective of a disease phenotype, an important consideration in our assessment of the impact of gene editing on the target ATXN1 transcript in B05 mice.

We next assessed editing efficiency *in vivo* in B05/ROSA-Cas9 mice or by co-delivery of AAV-Cas9 into B05 mice. Transgenes expressing gRNAs and/or Cas9 (Figure 2D) were packaged into rAAV1 and delivered via intra-cerebroventricular (ICV) injections into postnatal day 0 (P0) neonatal pups at a dose of 1E−10 viral genomes (vg) (Figure 2E). The B05/ROSA-Cas9 mouse expresses *Sp*Cas9 ubiquitously downstream of the CAG promoter.[29] Dual gRNA delivery did not result in *ATXN1* mRNA reduction compared to control (Figure 2F). In contrast, single gRNA delivery reduced *ATXN1* levels by 22% (Figure 2F). As the ROSA-Cas9 mouse is

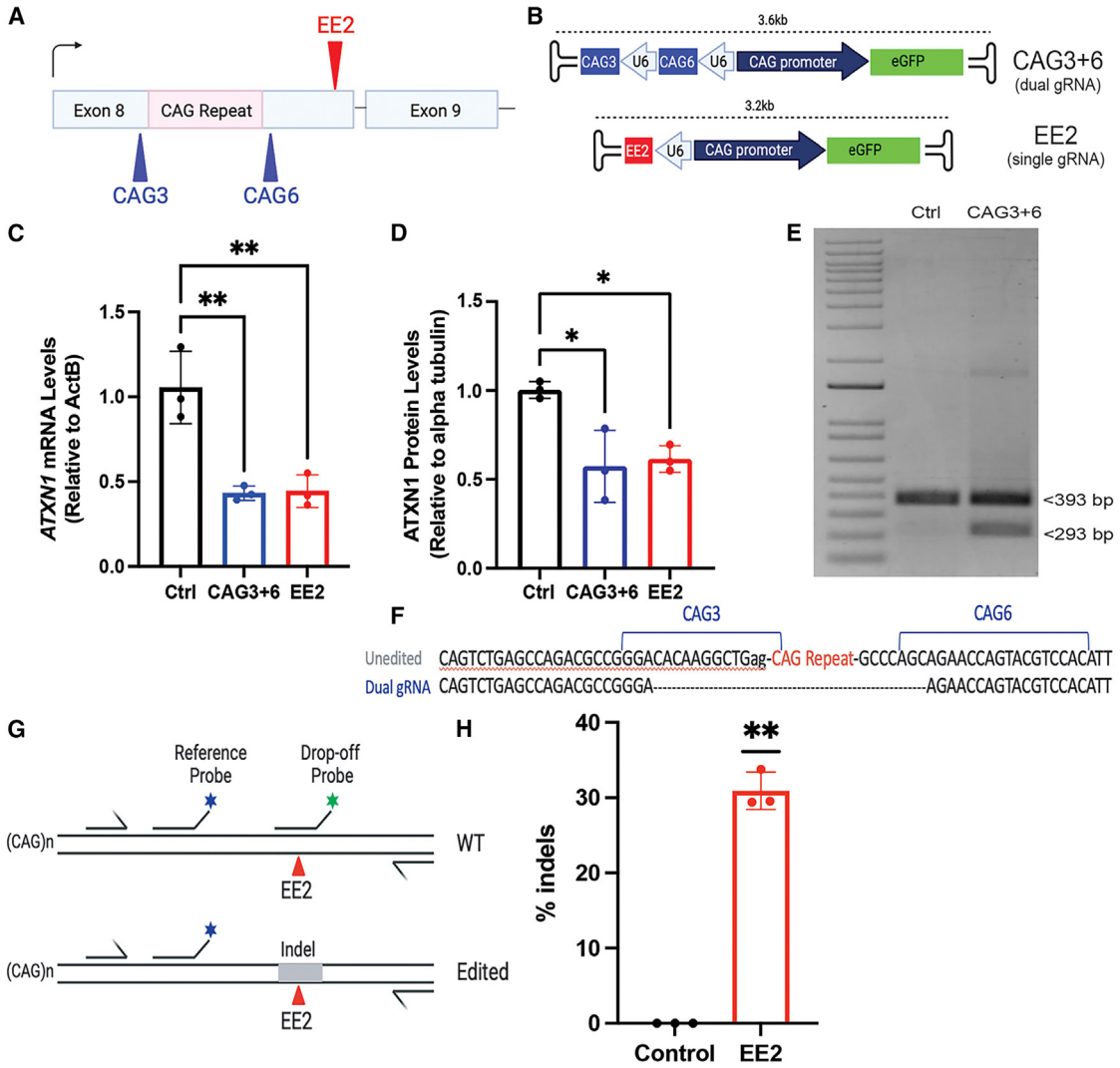

Figure 1. Dual and single gRNA strategies edit *ATXN1* *in vitro*

(A) Schematic of gRNA targeting sites for *ATXN1*. The single-guide strategy (EE2) targets at the EEJ between exon 8 and 9 and the dual-guide strategy (CAG3+6) targets both before and after the CAG repeat. (B) Diagram depicting the expression cassettes for single and dual gRNA strategies. gRNAs are driven by U6 promoters, and EGFP is expressed under a CAG promoter. mRNA (C) and protein (D) ATXN1 levels after single and dual gRNA transduction of HEK293-Cas9 cells. (E) Agarose gel following PCR assay surrounding the dual gRNA sites. Unedited cells have a single band at 393 bp, and a full CAG deletion caused by dual gRNA editing is seen in treated cells at 293 bp. (F) Sanger sequencing of extracted bands confirms full-length CAG deletion. (G) Schematic of ddPCR drop-off assay to assess indel formation. The reference probe binds to both edited and unedited (WT) DNA, and the drop-off probe cannot bind to ATXN1 DNA containing indels induced by Cas9 editing. (H) Indels calculated from ddPCR drop-off assay from transfected HEK293-Cas9 cells. Cells were sorted for EGFP and DNA collected from the positive population.Data in (C)–(E) represent mean ± SD, and significance was calculated with one-way ANOVA (C and D) or a one-sample t test (F); $^{*}p = 0.01$; $^{**}p = 0.002$.

not translatable to a clinical setting, we injected a 1:1 ratio of Cas9 and gRNA expressing AAVs in B05 mice. Co-AAV delivery into B05 mice resulted in an *ATXN1* reduction of 36% and 54% for dual and single gRNAs, respectively (Figure 2F). The increased efficacy is intriguing, given that the transcript levels of *Sp*Cas9 in mice treated via the co-AAV approach, or with Cas9 expressed transgenically, showed no difference in overall Cas9 transcript levels in the cerebellum (Figure 2G). Based on this, further studies were done using the co-AAV delivery approach.

Dual gRNA editing assessments in B05 mice and induced pluripotent stem cell neurons derived from SCA1 patients

AAV transduction of the cerebella results in PC transduction, with limited transduction of the more numerous granule cells.[30] This is beneficial when assessing target engagement (mRNA levels) of PC resident transcripts. However, to assess genomic outcomes of editing, a greater enrichment of edited genomes is required. Therefore, AAVs expressing gRNAs and Cas9 were injected into B05 striata, a site robustly transduced by AAV1. Tissues were harvested and amplicon

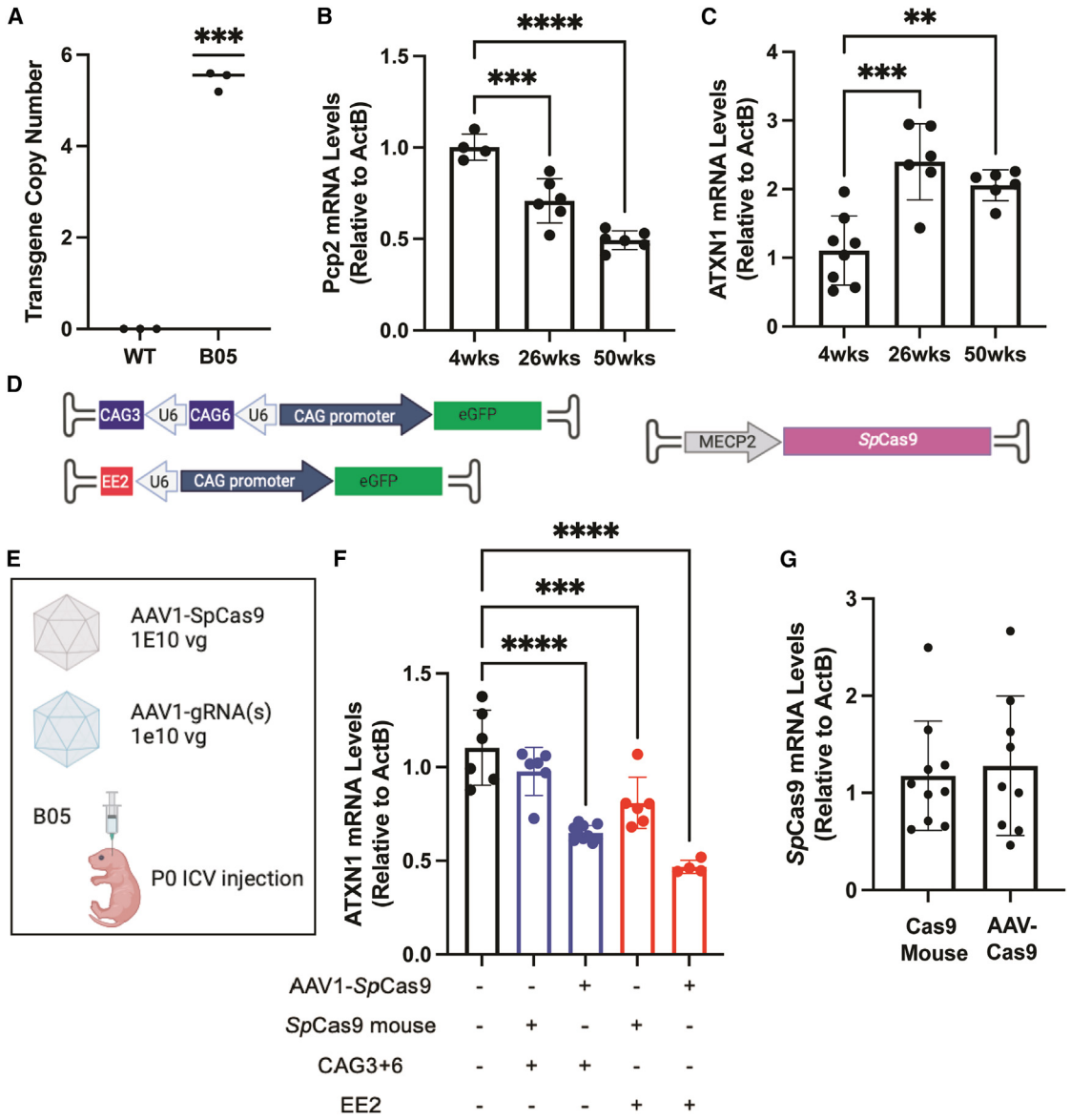

Figure 2. Analysis of B05 mouse model and *in vivo* editing of *ATXN1*

(A) ddPCR analysis of copy number of h*ATXN1* transgene in the B05 mouse. $n = 3$ hemizygous B05 mice. (B) *Pcp2* and (C) h*ATXN1* expression in B05 mouse cerebellum across ages. (D) Schematics of transgenes packaged into rAAV1. gRNAs are driven by U6 promoters, and EGFP is expressed under a CAG promoter. *Sp*Cas9 is expressed with a neuronal specific promoter, MECP2. (E) Diagram of injection strategy, rAAV1 delivered to P0 pups via ICV injection. AAV1 containing *Sp*Cas9 or gRNAs was delivered in a 1:1 ratio at a dose of 1E−10 vg. (F) Cerebellar *ATXN1* RNA knockdown in B05 mice 4 weeks post-injection for dual and single gRNA strategies to compare editing efficiencies of the ROSA-*Sp*Cas9 mouse and *Sp*Cas9 delivered via rAAV1. (G) Expression of *Sp*Cas9 mRNA in the cerebellum of 4-week-old mice from ROSA-Cas9 mice crossed to the B05 line and from B05 mice injected with AAV-Cas9. Significance in (A) was calculated with a one-sample t test; $^{***}p = 0.0005$. Data in (B), (C), and (F) represent mean ± SD, and significance was calculated with one-way ANOVA; $^{***}p < 0.001$; $^{****}p < 0.0001$.

nanopore sequencing performed (Figure 3A). In dual gRNA-injected mice, multiple reads containing CAG deletions ranging from 225 to 536 bp were detected (Figures 3B, 3C, and S5), with 0.5% of total reads containing a full CAG deletion (Figure 3D). Previous studies examining CRISPR deletions reported a deletion frequency of between 1% and 4%.[23] Of deletions that span the CAG repeat, 56% were 313 bp in length, which corresponds to the correct gRNA cut sites of CAG3+6 (Figure 3C). In uninjected B05 mice, multiple reads contained a variety of small deletions corresponding to potential base calling errors when sequencing through a repetitive area; however, there were no reads with deletions spanning the CAG repeat (Figure S5A).

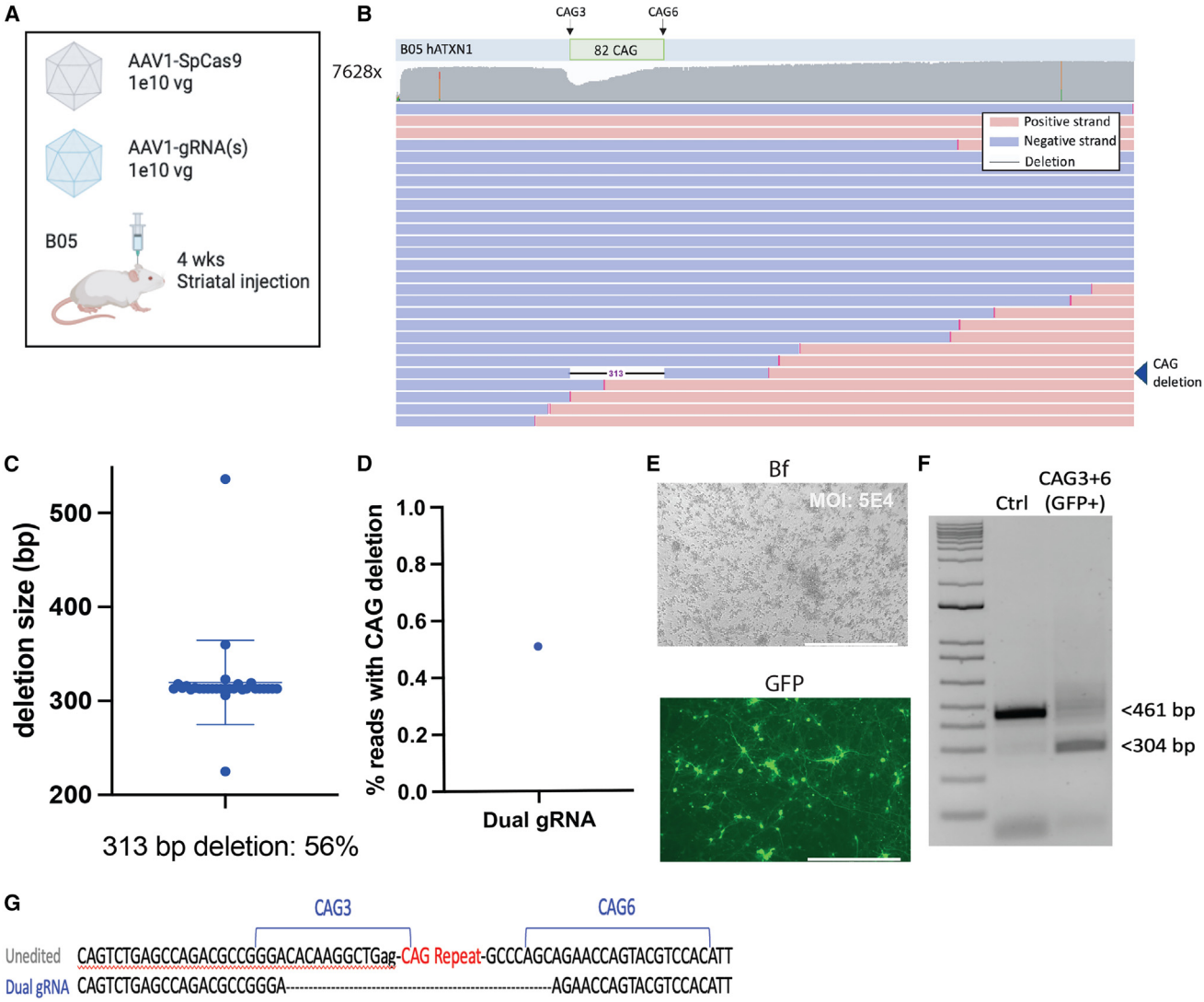

Figure 3. Dual gRNA editing assessments in B05 mice with nanopore sequencing and in iPSC neurons

(A) Diagram showing injection strategy for nanopore sequencing; adult hemizygous B05 mice injected with a 1:1 ratio of AAV-Cas9 and AAV-gRNAs directly into the striatum. (B) Representative IGV read pile-up of dual gRNA-injected mouse aligned to the human ATXN1 transgene. IGV plots were cropped to highlight relevant data; coverage is in gray; maximum base coverage is on the left; positive strands are red, negative strands are blue; and reads with intended CAG deletion are shown with the blue arrowhead. gRNA cut sites are represented by black arrows. (C) Deletion size from reads containing full CAG deletions (spanning the CAG repeat) in dual gRNA B05 mouse. Each dot represents a read containing a CAG deletion. (D) Frequency of reads with a deletion spanning the CAG repeat ($n = 30$). Full deletions were manually counted and ranged from 225 to 536 bp. (E) Transduction of AAV-Cas9 and AAV-gRNAs at a 1:1 ratio into SCA1 patient-derived iPSC neurons (MOI = 5E−4). Scale bar, 400 nm. (F) Agarose gel depicting PCR assay results with primers flanking the dual gRNA cut sites. Cells were flow sorted, and DNA from the EGFP$^+$ population was collected for analysis. Unedited cells (Ctrl) have a single band at 461 bp, and a full CAG deletion caused by dual gRNA editing is seen in treated cells at 304 bp. (G) Sanger sequencing of the edited band confirms full CAG deletion.

Next, we assessed editing in SCA1 patient induced pluripotent stem cells (iPSCs) and unaffected matched sibling donors. iPSCs were differentiated into neuronal progenitor cells (NPCs), and following quality control of SCA1 iPSC-derived inhibitory neurons, the 11–036 patient line and the matched control, 11–039, were used. We confirmed that the 11–036 line contains 2 *ATXN1* alleles with CAG repeat lengths of 30 and 41, while 11–039 has repeat lengths of 30 (Figure S6). *Sp*Cas9 and dual gRNA transgenes (Figure 2D) were packaged in AAVs and delivered to iPSC-derived neurons (Figure 3E). At 16 days post-transduction, cells were harvested and EGFP$^+$ cells visualized and sorted for DNA editing analysis (Figure 3F). Sequencing of PCR-amplified genomic DNA showed correct editing with a full CAG deletion noted in SCA1 patient iPSC neurons (Figure 3G). Next, off-target editing was assessed for the single gRNA

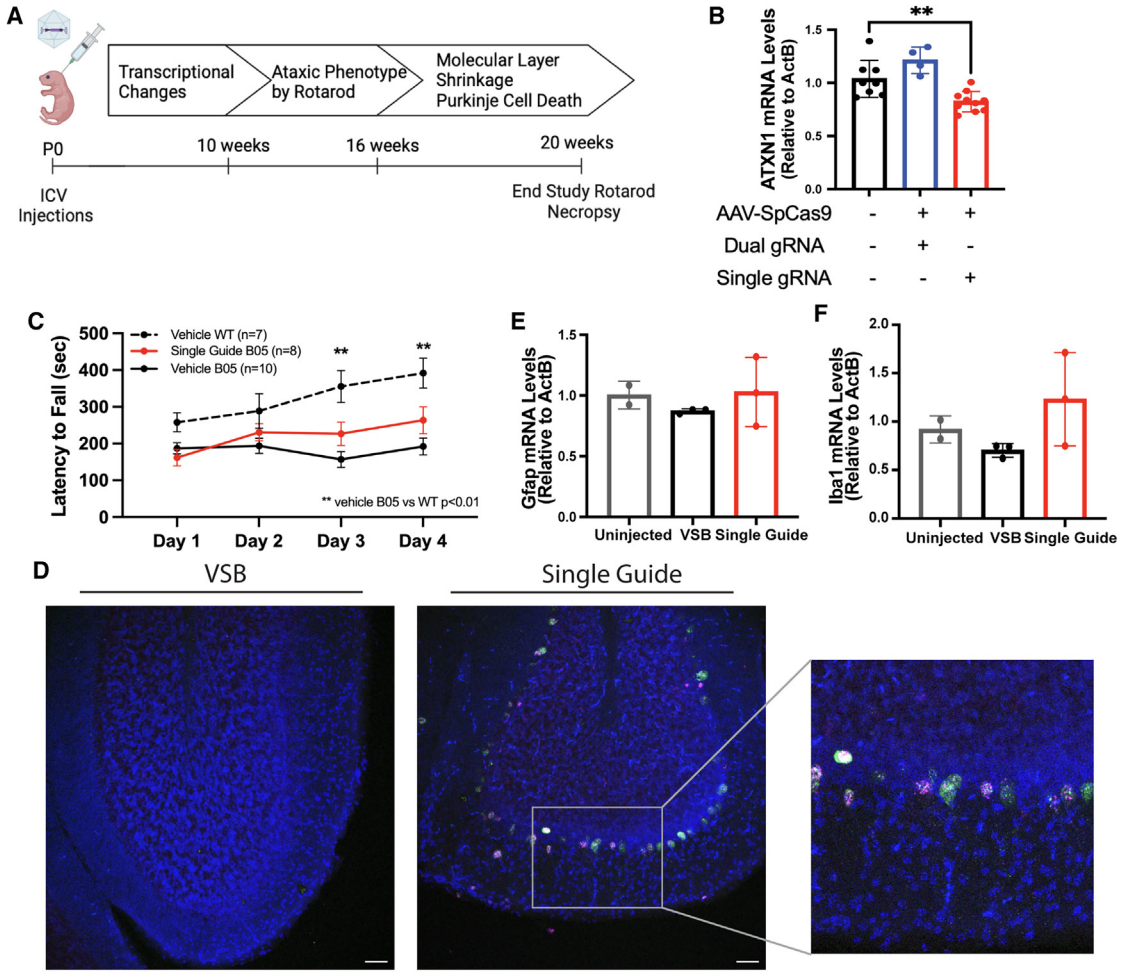

Figure 4. Single gRNA editing effects on behavior and tissue histology

(A) Outline of time line for behavior study. Hemizygous B05 pups were injected at P0 with an ICV injection of AAV1-Cas9 and AAV1-gRNA(s) at 7.5E−9 vg. At 20 weeks post-injection, animals were assessed on an accelerated rotarod for motor coordination, and at 25 weeks, tissue was collected. (B) *ATXN1* RNA knockdown 4 weeks post-P0 ICV injection (1:1 ratio of AAV-Cas9 and AAV-gRNA) in B05 mice with a dose of 7.5E−9 vg. Data represent mean ± SD, and significance was calculated with one-way ANOVA; $^{**}p < 0.007$. (C) Accelerated rotarod analysis of 20-week-old mice following treatment with vehicle (VSB) or single gRNA. Mice are tested for 4 consecutive days, and time on the rotarod (latency to fall) was measured. Statistical differences between groups were determined by mixed-effects analyses followed by Holm-Sidak's multiple comparisons test. (D) RNA-FISH depicting EGFP (green) and *Sp*Cas9 (red) expression in PCs of the cerebellum at 25 weeks. (E and F) qPCR analysis of RNA levels of *Gfap* (E) and *Iba1* (F) in 25-week-old mice.

strategy, first in HEK293-Cas9 cells. DNA was collected from control and single gRNA-treated EGFP$^+$ cells, and top off-target sites identified *in silico* were amplified and sequenced. The resultant data for the on-target site demonstrated high congruency with our ddPCR indel analysis and showed essentially no indel formation at these sites; 0.087% and −0.002% for predicted Off Target 1 and Off Target 2, respectively (Figure S7). Because of minimal off-target activity, further off-target analyses in iPSC cells were not done.

Single gRNA Cas9 editing improves behavior readouts

In B05 mice, disease progression results in decreased latency to fall on the accelerating rotarod by approximately 10 weeks of age compared to WT littermates.[7] This motor phenotype continues to deteriorate over time as PCs in the cerebellum degenerate beginning around 16 weeks. We therefore used this well-established model to assess the impact of gene editing on behavior. B05 pups were injected at P0 via ICV injections, and cerebellar RNA was collected 4 weeks post-injection to confirm knockdown (Figure 4A). At this dose (7.5E−9 vg), there was no difference in h*ATXN1* levels between the dual gRNA-treated animals and vehicle-injected B05 mice; however, in the single gRNA-injected B05 mice, h*ATXN1* levels were decreased by 20% (Figure 4B). Therefore, we moved forward to assess the impact of single gRNA treatment in B05 mice. At 20 weeks of age, mice were assessed for motor coordination on the accelerated rotarod. As expected, control treated B05 mice displayed significantly decreased latency to fall compared to WT littermates (Figure 4C).

Single gRNA-injected B05 mice were improved over vehicle-treated B05 animals (Figure 4C), showing a partial behavior rescue of the SCA1 phenotype with the single gRNA strategy. As current literature suggests a 30% reduction of *ATXN1* is necessary for complete behavior and pathological correction, a partial rescue on the rotarod correlates as expected with our observed 20% reduction in h*ATXN1* mRNA.[31] Following necropsy at 25 weeks, RNA fluorescence *in situ* hybridization (RNA-FISH) was used to assess transduction by visualizing EGFP and *Sp*Cas9 within the cerebellum. In single gRNA-injected B05 mice, there was strong expression of both EGFP and Cas9 throughout the PCs in the cerebellum (Figure 4D).

Persistent *in vivo* expression of *Sp*Cas9 and EGFP via AAV have been shown to elicit an immune response.[32,33] To assess potential inflammation, glial fibrillary acidic protein (Gfap; a marker of astroglia activation) and ionized calcium-binding adapter molecule 1 (Iba1; a marker of microglial activation) were assessed in cerebellar tissues. Both histological staining and mRNA levels of Gfap and Iba1 were not increased in treated mice over vehicle-injected mice (Figures 4E, 4F, S8A, and S8B). This indicates that neither the route of administration, the AAV itself, nor the Cas9 cargo resulted in increased inflammation. In combination, these data present a potential therapeutic avenue that reduces motor coordination deficits in SCA1 mice and does not induce inflammation.

DISCUSSION

There are currently no disease-modifying treatment options available for SCA1, resulting in an unmet need in this community. Gene editing with Cas9 presents an opportunity for treatment for both this disease and many other neurodegenerative diseases caused by a triplet repeat expansion, such as HD or myotonic dystrophy.[26,27,34] However, before these treatments can be used clinically, a deeper understanding of both efficacy and editing events is necessary. This study shows Cas9 editing in various model systems.

Transgenic animal models are incredible tools for studying disease and gene function. However, many of the intrinsic features of these models introduce variables that make pre-clinical studies, particularly those involving DNA editing, difficult to interpret and translate into therapies. Transgenic mice have most commonly been generated by microinjecting a transgenic construct into a fertilized egg, resulting in offspring that may contain multiple stochastically integrated transgene copies.[35,36] We found that the B05 heterozygote contained 5 transgene copies, down from the original report of 25–30.[6] The B05 mouse contains 2.5 times as many gRNA binding sites/copies of the *ATXN1* sequence compared to humans, which could reflect a higher level of required Cas9 editing to elicit more robust knockdown. The multiplicity of transgenes also complicates editing event analysis. We found with nanopore sequencing that dual gRNA-treated mice contain less than 1% of reads with a full CAG deletion (Figure 3C). Since deletions require near-simultaneous cleavage at both gRNA cut sites, the opportunity for this may be further reduced upon the introduction of additional gRNA cut site locations within the genome.[23] As the B05 mice have five additional sites for the gRNAs to bind and cleave, successful deletions are therefore more difficult to obtain. The position of transgene copies within a genome can also complicate editing analysis as tandem transgene copies can result in large deletions following editing due to the amalgamation of tandem transgenes.[23] While this possibility is not relevant in clinical settings, it further complicates editing analysis in transgenic animals.

We assessed editing in B05 mice with both the ROSA-Cas9 mouse and with AAV-delivered Cas9. We found that while there is no significant difference in total Cas9 expression, the AAV-delivered Cas9 elicited a 30% greater reduction of h*ATXN1* compared to the ROSA-Cas9 mouse (Figure 2F). We hypothesize that the cell-specific expression of the *ATXN1* transgene may be responsible for this disparity. Expression levels of Cas9 were measured based on whole cerebellar lysates, and cell-specific expression in the CNS has not been investigated in the ROSA-Cas9 mouse. Endogenous expression of Cas9 in cells of the cerebellum that do not express the transgene, such as granule cells, may be higher than in PCs. Therefore, while overall cerebellar expression is the same as AAV-Cas9, PC expression of Cas9 may be significantly lower, resulting in lower editing efficiency. This could be further investigated using RNA-FISH to assess expression within cell types; however, due to the limited translatability of the ROSA-Cas9 mouse, we chose to move forward with AAV-Cas9.

The cell-specific expression of *ATXN1* cDNA in the B05 mouse is also important to consider regarding editing outcomes. Since this mouse model expresses cDNA, there is no intron present, and thus no splicing occurs.[6] Therefore, the induction of NMD by targeting the EEJ is not relevant in this mouse model, and editing outcomes could therefore be drastically different compared to human cells that do undergo splicing. Cas9 editing in the B05 mouse may cause a frameshift at the *ATXN1* locus, resulting in the formation of a premature termination codon that undergoes NMD without the presence of an intron.[37] The cell-specific expression is also restricted in the B05 model and likely accounts for the increased *ATXN1* levels across ages (Figure 2C). A more translationally relevant model for SCA1 was recently released, the Q146 model, while our work was under way.[28] This knockin mouse model expresses h*ATXN1* ubiquitously with 146 polyQ repeats from the endogenous mouse *Atxn1* locus. In early work assessing this model, we found that cerebellar *Pcp2* and *ATXN1* transcript levels decrease with age, as expected (Figure S3). This indicates that the increased *ATXN1* levels observed in the B05 mouse are not indicative of a disease phenotype. In future studies we will explore the impact of editing outcomes in the Q146 model; presently, the model was useful in helping ascertain the relevance of the changes in PC-gene expression over time in the B05 model.

Here, iPSC-derived neurons allowed assessment of editing efficiencies of Cas9-based therapies. SCA1 patient-derived iPSC neurons have been shown to recapitulate various aspects of disease phenotypes such as protein aggregates, dendrite shortening, and reduced branching, as well as transcriptomic changes.[38] In our study, we differentiated SCA1 patient iPSCs into inhibitory neurons,

one of the primarily affected cell types in SCA1. There are many transcriptional changes that occur pre-symptomatically in SCA1, so the ability to both transduce patient iPSCs with rAAV and to induce edits via CRISPR are important steps regarding future translatability. In this study, we initially focused on confirming the ability to transduce patient iPSCs and induce Cas9 cleavage; future studies will further investigate editing events and rescue following treatment.

Currently, one possible therapeutic strategy for SCA1 is the use of RNAi to target the *ATXN1* transcript for knockdown. This has been shown to prevent and reverse SCA1 phenotypes after disease onset in mice. The key drawbacks of RNAi as a therapeutic, reliance on endogenous machinery and the requirement for continuous expression, can be circumvented by Cas9 editing.[20,39–42] Genome editing using Cas9 utilizes an exogenous enzyme and provides an alternative to continual expression, as once an edit has been made, the presence of the Cas9 enzyme is no longer necessary. Extended expression of the Cas9 protein increases the probability of both off-target editing and toxicity so a burst of short-lasting expression is ideal.[43,44] The use of a "switch" system has been used in HD to induce editing using an orally available, CNS-penetrant drug, branaplam.[45,46] This allows for a burst or bursts of Cas9 expression only following drug administration. This decreases the possibility of off-target editing and of inflammation arising from the expression of a bacterial protein, Cas9.[33] The approach used in this paper is not allele specific and targets both WT and mutant ATXN1 for Cas9-mediated knockdown. ATXN1 functions in the cell as a transcriptional repressor through the interaction with multiple binding partners. ATXN1L shares 33% homology with ATXN1, including the AXH domain, which facilitates the interaction of both ATXN1 and ATXN1L with CIC.[47] The shared domain and binding partners between these proteins allows for functional redundancy; however, the gRNAs currently use only target ATXN1 for knockdown. This allows us to target both WT and mutant ATXN1 with our Cas9 strategies and maintain required cellular function regardless of ATXN1 reduction. Our study demonstrates a proof-of-concept for Cas9-mediated protection in SCA1. In summary, we present data showing the utility of CRISPR-based editing approaches for SCA1 in mice models and in patient-derived cells, adding another tool to the various gene therapy modalities available for advancing SCA1 treatments.

MATERIALS AND METHODS

Cell culture and transfection

HEK293 cells (obtained from Children's Hospital of Philadelphia [CHOP] Research Vector Core stock) were maintained in DMEM media containing 10% fetal bovine serum, 1% L-glutamine, and 1% penicillin/streptomycin at 37°C with 5% CO_2. Cells were cultured in 24-well plates and transfected at 80%–90% confluence using Lipofectamine 3000 transfection reagent, according to the manufacturer's protocol. Cells were not authenticated or tested for Mycoplasma by the investigators since they previously passed the quality controls of the CHOP Research Vector Core.

sgRNA and Cas9 plasmid construction

The pX330 plasmid was provided by Dr. Feng Zhang and modified to contain both EGFP/puromycin resistance, as previously described.[25] gRNA sequences were cloned with a pair of complementary oligonucleotides into the Bbsl cloning site and driven by the hU6 promoter. This plasmid was used for initial screening of gRNAs, after which best-candidate gRNAs from the dual- and single-guide strategies were cloned into a AAV shuttle plasmid using gBlock assembly. The px551 plasmid (Addgene, catalog no. 60957) was used *in vivo* for *Sp*Cas9 expression.

gRNA screen into HEK293 cells and confirmation in HEK293-Cas9 cells

HEK293 cells were cultured into a 24-well plate and transfected at roughly 80% confluency with pX330 plasmids containing gRNAs. At 48 h following transfection, cells underwent a puromycin selection for 24 h, and cells were collected for RNA isolation. HEK293 cells expressing Cas9 were used with the pKAAV-gRNA(s) plasmids to confirm efficacy. Cells were cultured in a 24-well plate and transfected at 80% confluency. At 48 h following transfection, cells were collected for RNA and DNA isolation. For the ddPCR drop-off assay and off-target amplicon sequencing, cells were collected in fluorescence-activated cell sorting (FACS) buffer (250 mg BSA, 0.5M EDTA, 50 mL PBS) and flow sorted on the Aurora CS-1 Spectral Sorter. $EGFP^+$ cells were collected for DNA extraction.

Genomic DNA extraction and ddPCR assays

Genomic DNA was extracted using a DNeasy Blood and Tissue Kit (QIAGEN, catalog no. 69504) according to the manufacturer's instructions. ddPCRs were performed on the QX200 (Bio-Rad) according to the manufacturer's instructions. A total of 100 ng DNA was used for drop-off assays, and the QX Manager Software (Bio-Rad, version 1.2) was used for analyzing indel formation (Table S3). For assessing transgene copy number the *Tfrc* reference assay (Thermo Fisher Scientific, catalog no. 4458366) was used with the h*ATXN1* (Hs00165656_m1) probe with 50 ng DNA.

RNA extraction, qRT-PCR of *ATXN1*, Pcp2, calbindin expression levels

Total RNA was extracted using Trizol (Thermo Fisher, catalog no. 15596026) according to the manufacturer's protocol and quantified by spectrophotometry. RT-qPCR measurements were made using a CFX384 Real Time System from Bio-Rad on samples prepared using TaqMan Universal Master Mix II, no UNG (Applied Biosystems), with TaqMan primer/probe sets directed against h*ATXN1* (Hs00165656_m1), mouse *IbaI* (Mm00479862_g1), mouse *Gfap* (Mm01253033_m1), mouse β-*actin* (4352341E), mouse *Atxn1* (Mm00485928_m1), mouse *Pcp2* (Mm00435514_m1), mouse *Calb* (Mm00486647_m1), and human β-*actin* (Hs01060665_g1).

Western blot analysis

HEK293 cells seeded in 24-well plates were resuspended in 200 μL radioimmunoprecipitation assay buffer (50 mM Tris-HCl, pH 8, 150 mM NaCl, 1% Triton X-100, 0.5% sodium deoxycholate, 0.1% SDS)

supplemented with 1× cOmplete Protease Inhibitors (Roche). Samples were incubated on ice for 30 min and then spun at >18,000 × *g* for 20 min at 4°C. The supernatant protein concentration was measured using a DC Protein Assay Kit II (Bio-Rad). A total of 25 μg was loaded into 4%–12% Criterion XT Bis-Tris gels (Bio-Rad) and transferred to polyvinylidene fluoride membranes for blotting. Membranes were blocked for 1 h at room temperature in 5% milk in 1× TBST (137 mM NaCl, 2.7 mM KCl, 19 mM Tris base, 0.1% Tween 20). Rabbit anti-ATXN1 11NQ was diluted 1:2,000 in 2% BSA in TBST and incubated overnight at 4°C followed by goat anti-rabbit immunoglobulin G horseradish peroxidase (IgG HRP) (Thermo Fisher) diluted 1:10,000 in 5% milk in TBST. Membranes were exposed using ECL Prime Western Blotting Detection Reagent (Cytiva). Without stripping, blots were reprobed using mouse anti-alpha tubulin Clone B-5-1-2 (Thermo Fisher) diluted 1:10,000 in 5% milk TBST overnight at 4°C followed by secondary goat anti-mouse IgG HRP (Thermo Fisher) 1:10,000 in 5% milk.

rAAV vector design and production

For *in vivo* studies, three different rAAV vectors were generated: one expressing *Sp*Cas9 and two containing the gRNA cassettes with EGFP. Viruses were generated by the Research Vector Core at the Raymond G. Perelman Center for Cellular and Molecular Therapeutics at CHOP. *Sp*Cas9 was expressed under the control of a minimal cytomegalovirus (CMV) immediate-early gene enhancer/promoter region (CMV promoter) and cloned upstream of a minimal poly A sequence (FBAAV-Cas9). The gRNA expression cassettes were moved into an AAV shuttle plasmid containing an EGFP gene under the control of the CAG promoter and upstream of an SV40 polyadenylation signal. All rAAV plasmid shuttles have AAV2 inverted terminal repeat sequences. rAAV vectors were produced by the standard calcium phosphate transfection method in HEK293 cells by using the AdHelper, AAV1 *trans*-packaging, and AAV shuttle plasmids. Vector titers were determined by ddPCR, and vector purity was also tested by Ag staining.

Targeted amplicon sequencing for off-target analysis

Identification of potential off-targets by Cas-OFFinder (http://www.rgenome.net/cas-offinder/) was done, allowing two mismatches and up to two DNA/RNA bulges. Genomic DNA from HEK-Cas9 cells (single gRNA transfected and control transfected) was amplified at sites identified (Table S4) using primers noted in Table S2. Sites were analyzed and visualized using CRISPResso2.

Mouse studies

All animal protocols were approved by the CHOP Animal Use and Care Committee. B05 mice were developed by Dr. H.T. Orr at the University of Minnesota, were re-derived by The Jackson Laboratories in 2014 and are maintained on a pure FVB background. ROSA-Cas9 mice were obtained from Jackson Laboratories (Jax Stock, catalog no. 024858) and maintained on FVB background.[29] Q146 mice were generously provided by Dr. H.T. Orr and maintained on C57B/6 background. All study animals were obtained from litters derived from breeding hemizygous positive B05 males with WT FVB females from The Jackson Laboratories or with ROSA-Cas9 females. All animals used in this study were hemizygous B05 and hemizygous ROSA-Cas9 mice. Genotypes were determined by qPCR for the mutant transgene. Animals were housed in a climate-controlled environment and kept on a 12-h light/dark cycle with access to food ad libitum.

AAV injection and tissue isolation

Mice were injected at either P0 with an ICV injection or at 4 weeks of age into the striatum. For adult injections, mice were anesthetized with isofluorane and injected 1:1 of rAAV2/1-*Sp*Cas9 and rAAV2/1-U6gRNA/EGFP virus. A total of 8 μL (4 μL per hemisphere) of rAAV mixture was injected bilaterally into the striatum at 220 nL/min (coordinates: +0.86 mm rostral to bregma, 1.8 mm lateral to medial, and 2.5 mm ventral from brain surface). Neonatal mice were anesthetized on ice and 4 μL total (2 μL per hemisphere) of the rAAV mixture was injected (three-fifths the distance between bregma and the eye to a depth of 2 mm) to target the ventricles.[48] After 4 weeks (25 weeks for the behavior study) mice were anesthetized with a ketamine and xylazine mix and perfused with 20 mL cold PBS. The brains were then removed, flash frozen in liquid nitrogen, and stored at −80°C until use. For staining, brains were placed in 4% paraformaldehyde (PFA) for 24 h before transferring to a 30% sucrose solution.

gDNA preparation for nanopore sequencing

Frozen striatum samples were ground with a pestle in lysis buffer, and gDNA was extracted using the DNA genomic-tip kit (QIAGEN, catalog no. 13343). gDNA, 100 ng, was PCR amplified with PrimeStar HS DNA Polymerase (Takara, catalog no. R010A) (Table S2) and purified using the QIAquick PCR Purification Kit (QIAGEN, catalog no. 28104). Concentrations were quantified using the Qubit fluorometer (Thermo Fisher Scientific).

PCR-amplified library preparation for nanopore sequencing

A total of 200 fmol gDNA was dA-tailed using dATP and Taq polymerase (NEB, catalog no. M0273) by incubation at 37°C for 30 min, then 72°C for 5 min, and held at 4°C. Samples were cleaned with a 1:1 ratio of AMPure XP beads (Beckman Coulter, catalog no. A63881) and washed twice with 70% ethanol and eluted with nuclease-free water. Adapter ligation was performed with the ligation sequencing kit (Oxford Nanopore Technologies, catalog no. SQK-LSK110) using NEBNext Quick T4 DNA Ligase (NEB, catalog no. E6056) by incubation at room temperature for 10 min. gDNA was then cleaned again with 0.4× volume of AMPure XP beads and washed with short fragment buffer (Oxford Nanopore Technologies, catalog no. SQK-LSK110). The library was eluted in 7 μL elution buffer (Oxford Nanopore Technologies, catalog no. SQK-LSK110).

Nanopore sequencing

The sequencing library was prepared with 5.5 μL DNA library, 13.5 μL sequencing buffer II (Oxford Nanopore Technologies, catalog no. SQK-LSK110) and 11 μL loading beads II (Oxford Nanopore Technologies, catalog no. SQK-LSK110). Flow cell priming mix was

prepared with 3 μL flush buffer (Oxford Nanopore Technologies, catalog no. SQK-LSK110) and 117 μL flush tether (Oxford Nanopore Technologies, catalog no. SQK-LSK110). Libraries were loaded onto the R9.4.1 Flongle flow cells (Oxford Nanopore Technologies, catalog no. FLO.FLG001).

Nanopore sequencing analysis

Raw FAST5 sequencing files were base called with Guppy (version 5.0.7) using a minimum read quality threshold of Q score of 7 to generate passed FASTQ reads and aligned using MiniMap2 (version 2.17-r941) to create BAM files. Alignments were made to a reference genome that included the human *ATXN1* transgene. Total reads and aligned reads were determined with samtools (version 1.10-2) using BAM files. Read alignments were viewed using the Integrative Genomics Viewer (IGV) (version 2.16.2) for manually counting full CAG deletions.[49]

iPSC culturing and analysis

SCA1 patient iPSCs were generously provided by Dr. H.T. Orr after collection, as detailed previously.[50] The CHOP Research Institute Human Pluripotent Stem Cell Core differentiated the patient iPSCs to NPCs as described,[51] and 300,000 cells per well were plated in a 24-well plate. At 40 days post-differentiation, iPSC-derived neurons were transduced with AAV at an MOI of 5E−4 by removing half of the existing media and replacing it with fresh media containing AAV-*Sp*Cas9 and AAV-gRNAs. Half-media changes were performed every other day until day 16 post-transduction, when cells were rinsed with PBS and dissociated using TrypLE (Thermo Fisher, catalog no. 12604013). Media was then added to neutralize the TrypLE, and cells were pelleted by spinning at 300 rpm for 5 min. Cell pellets were resuspended in 300 μL FACS buffer (0.5% BSA, EDTA [2 mM] in PBS), and using the FACSJazz (BD Biosciences), cells were sorted into an $EGFP^+$ population and collected into Eppendorf tubes. DNA was extracted using a DNeasy Blood and Tissue Kit (QIAGEN) according to the manufacturer's instructions and PCR amplified with PrimeStar HS DNA Polymerase (Takara, catalog no. R010A) (Table S2).

Accelerating rotarod

Mice were tested on an accelerating rotarod apparatus at 20 weeks of age. Mice were first habituated on the rotarod for 5 min. Mice were then tested 3 trials per day (with at least 30 min of rest between trials) for 4 consecutive days. For each trial, acceleration was from 4 to 40 rpm over 5 min, and then speed maintained at 40 rpm. Latency to fall (or if mice hung on for two consecutive rotations without running) was recorded for each mouse per trial. The trials were stopped at 500 s, and mice remaining on the rotarod at that time were scored as 500 s. Two-way ANOVA was used to assess for significant differences.

Histology

Fixed brains were mounted in Optimal Cutting Temperature (OCT) and cut to a thickness of 40 μm using a Leica CM1950 cryostat. Free-floating sections were stored in cryoprotective media (30% w/v sucrose, 30% v/v ethylene glycol, 0.1 M phosphate buffer) at −20°C. Washes were done six times for 5 min in dilution media (0.1% Tris Base, 0.0002% NaCl, and 0.2% Triton X-100) to remove OCT. Sections were later blocked in 10% goat serum in PBS at room temperature for 1 h. The following primary antibodies were used: 1:500 rabbit anti-calbindin-D-28K (Millipore, catalog no. C2724), 1:500 rabbit IBA-1 (Wako Chemicals, catalog no. 019–19741), and 1:1,000 rabbit GFAP (Dako, catalog no. 019–19741).

Sections were incubated in primary antibody (diluted in 3% goat serum and 0.2% Triton X-100 in PBS) overnight. After incubation, slides were washed in dilution media six times for 5 min, and then treated for 1 h with Alexa Fluor-conjugated secondary antibodies (Thermo Fisher, catalog no. 00-4958-02). Secondary antibodies were diluted with 3% goat serum and 0.2% Triton X-100 in PBS at 1:500 for anti-calbindin-D-28K, and 1:2,000 for GFAP and IBA-1. Slides were counterstained with Hoechst (1:5,000) for 5 min and then washed five times for 5 min with dilution media. Sections were mounted and the slides were coverslipped using Fluoromount-G mountant (Thermo Fisher). Images were taken using the Leica DM 6000 B episcope.

RNA-FISH

We processed 4% PFA-fixed brain slices with a RNAscope multiplex fluorescent reagent kit version 2 assay (Advanced Cell Diagnostics, catalog no. USM-323100) according to the manufacturer's instructions. In brief, endogenous peroxidases were inhibited by incubation with hydrogen peroxide for 10 min at room temperature. Tissue was moved into antigen retrieval solution at 95°C for 5 min, followed by washing with 100% ethanol for 3 min and air drying at room temperature. Before hybridization, protease III solution was incubated for 30 min at 40°C followed by two washes with double distilled H_2O. RNAscope probes for GFP-C2 transcripts were hybridized for 2 h at 40°C. Probe was developed with Opal 570 fluorophore (Akoya Biosciences, catalog no. FP1488001KT). Nuclei were labeled with Hoescht (1:5,000), and slides were mounted in mounting media (SouthernBiotech, catalog no. 0100-01).

Figure generation

Figures were made with Biorender.com and assembled on Adobe Illustrator or Adobe Photoshop after importing panels.

Statistical analysis

All statistical analyses were performed using GraphPad Prism version 10.0 software. All data with normal distribution were analyzed using one-way ANOVA followed by a Bonferroni's post hoc or an unpaired t test unless otherwise stated. Rotorod data were analyzed using a mixed-effects analysis followed by a Holm-Sidak's multiple comparisons post hoc test.

ACKNOWLEDGMENTS

The authors acknowledge Carolyn Yrigollen, PhD, for assistance with nanopore sequencing/analysis; Dominika Houserova, PhD, for Cas off-target analysis; and Jesse

Weber for editorial comments on the manuscript. This work was supported by the National Ataxia Foundation and the Children's Hospital of Philadelphia Research Institute.

AUTHOR CONTRIBUTIONS

Conceptualization: K.J.F., E.M.C., and B.L.D.; data acquisition: K.J.F., G.C., and E.A.W.; writing, review, & editing: K.J.F., E.M.C., G.C., and B.L.D.; resources and supervision: B.L.D.

DECLARATION OF INTERESTS

B.L.D. serves on the advisory board of Latus Biosciences, Spirovant Biosciences, Resilience, and Carbon Biosciences. She has sponsored research from Roche, Latus, and Saliogen.

SUPPLEMENTAL INFORMATION

Supplemental information can be found online at https://doi.org/10.1016/j.omtn.2024.102317.

REFERENCES

1. Banfi, S., Servadio, A., Chung, M.-y., Kwiatkowski, T.J., McCall, A.E., Duvick, L.A., Shen, Y., Roth, E.J., Orr, H.T., and Zoghbi, H.Y. (1994). Identification and characterization of the gene causing type 1 spinocerebellar ataxia. Nat. Genet. *7*, 513–520.
2. Crespo-Barreto, J., Fryer, J.D., Shaw, C.A., Orr, H.T., and Zoghbi, H.Y. (2010). Partial loss of ataxin-1 function contributes to transcriptional dysregulation in spinocerebellar ataxia type 1 pathogenesis. PLoS Genet. *6*, e1001021.
3. Duyckaerts, C., Dürr, A., Cancel, G., and Brice, A. (1999). Nuclear inclusions in spinocerebellar ataxia type 1. Acta Neuropathol. *97*, 201–207.
4. Orr, H.T., Chung, M.Y., Banfi, S., Kwiatkowski, T.J., Jr., Servadio, A., Beaudet, A.L., McCall, A.E., Duvick, L.A., Ranum, L.P., and Zoghbi, H.Y. (1993). Expansion of an unstable trinucleotide CAG repeat in spinocerebellar ataxia type 1. Nat. Genet. *4*, 221–226.
5. Skinner, P.J., Koshy, B.T., Cummings, C.J., Klement, I.A., Helin, K., Servadio, A., Zoghbi, H.Y., and Orr, H.T. (1997). Ataxin-1 with an expanded glutamine tract alters nuclear matrix-associated structures. Nature *389*, 971–974.
6. Burright, E.N., Clark, H.B., Servadio, A., Matilla, T., Feddersen, R.M., Yunis, W.S., Duvick, L.A., Zoghbi, H.Y., and Orr, H.T. (1995). SCA1 transgenic mice: a model for neurodegeneration caused by an expanded CAG trinucleotide repeat. Cell *82*, 937–948.
7. Clark, H.B., Burright, E.N., Yunis, W.S., Larson, S., Wilcox, C., Hartman, B., Matilla, A., Zoghbi, H.Y., and Orr, H.T. (1997). Purkinje Cell Expression of a Mutant Allele of SCA1in Transgenic Mice Leads to Disparate Effects on Motor Behaviors, Followed by a Progressive Cerebellar Dysfunction and Histological Alterations. J. Neurosci. *17*, 7385–7395.
8. Ingram, M., Wozniak, E.A.L., Duvick, L., Yang, R., Bergmann, P., Carson, R., O'Callaghan, B., Zoghbi, H.Y., Henzler, C., and Orr, H.T. (2016). Cerebellar Transcriptome Profiles of ATXN1 Transgenic Mice Reveal SCA1 Disease Progression and Protection Pathways. Neuron *89*, 1194–1207.
9. Keiser, M.S., Geoghegan, J.C., Boudreau, R.L., Lennox, K.A., and Davidson, B.L. (2013). RNAi or overexpression: alternative therapies for Spinocerebellar Ataxia Type 1. Neurobiol. Dis. *56*, 6–13.
10. Keiser, M.S., Monteys, A.M., Corbau, R., Gonzalez-Alegre, P., and Davidson, B.L. (2016). RNAi prevents and reverses phenotypes induced by mutant human ataxin-1. Ann. Neurol. *80*, 754–765.
11. Yue, S., Serra, H.G., Zoghbi, H.Y., and Orr, H.T. (2001). The spinocerebellar ataxia type 1 protein, ataxin-1, has RNA-binding activity that is inversely affected by the length of its polyglutamine tract. Hum. Mol. Genet. *10*, 25–30.
12. Lam, Y.C., Bowman, A.B., Jafar-Nejad, P., Lim, J., Richman, R., Fryer, J.D., Hyun, E.D., Duvick, L.A., Orr, H.T., Botas, J., and Zoghbi, H.Y. (2006). ATAXIN-1 interacts with the repressor Capicua in its native complex to cause SCA1 neuropathology. Cell *127*, 1335–1347.
13. Watase, K., Gatchel, J.R., Sun, Y., Emamian, E., Atkinson, R., Richman, R., Mizusawa, H., Orr, H.T., Shaw, C., and Zoghbi, H.Y. (2007). Lithium therapy improves neurological function and hippocampal dendritic arborization in a spinocerebellar ataxia type 1 mouse model. PLoS Med. *4*, e182.
14. Mellesmoen, A., Sheeler, C., Ferro, A., Rainwater, O., and Cvetanovic, M. (2018). Brain Derived Neurotrophic Factor (BDNF) Delays Onset of Pathogenesis in Transgenic Mouse Model of Spinocerebellar Ataxia Type 1 (SCA1). Front. Cell. Neurosci. *12*, 509.
15. Bushart, D.D., Chopra, R., Singh, V., Murphy, G.G., Wulff, H., and Shakkottai, V.G. (2018). Targeting potassium channels to treat cerebellar ataxia. Ann. Clin. Transl. Neurol. *5*, 297–314.
16. NIH (2019). Spinocerebellar ataxia type 1. https://ghr.nlm.nih.gov/condition/spinocerebellar-ataxia-type-1#.
17. Friedrich, J., Kordasiewicz, H.B., O'Callaghan, B., Handler, H.P., Wagener, C., Duvick, L., Swayze, E.E., Rainwater, O., Hofstra, B., Benneyworth, M., et al. (2018). Antisense oligonucleotide-mediated ataxin-1 reduction prolongs survival in SCA1 mice and reveals disease-associated transcriptome profiles. JCI Insight *3*, e123193.
18. Crooke, S.T. (2017). Molecular Mechanisms of Antisense Oligonucleotides. Nucleic Acid Ther. *27*, 70–77.
19. Carrell, E.M., Keiser, M.S., Robbins, A.B., and Davidson, B.L. (2022). Combined overexpression of ATXN1L and mutant ATXN1 knockdown by AAV rescue motor phenotypes and gene signatures in SCA1 mice. Mol. Ther. Methods Clin. Dev. *25*, 333–343.
20. Agrawal, N., Dasaradhi, P.V.N., Mohmmed, A., Malhotra, P., Bhatnagar, R.K., and Mukherjee, S.K. (2003). RNA interference: biology, mechanism, and applications. Microbiol. Mol. Biol. Rev. *67*, 657–685.
21. Cong, L., Ran, F.A., Cox, D., Lin, S., Barretto, R., Habib, N., Hsu, P.D., Wu, X., Jiang, W., Marraffini, L.A., and Zhang, F. (2013). Multiplex genome engineering using CRISPR/Cas systems. Science *339*, 819–823.
22. Jinek, M., Chylinski, K., Fonfara, I., Hauer, M., Doudna, J.A., and Charpentier, E. (2012). A programmable dual-RNA-guided DNA endonuclease in adaptive bacterial immunity. Science *337*, 816–821.
23. Simpson, B.P., Yrigollen, C.M., Izda, A., and Davidson, B.L. (2023). Targeted long-read sequencing captures CRISPR editing and AAV integration outcomes in brain. Mol. Ther. *31*, 760–773.
24. Dabrowska, M., Juzwa, W., Krzyzosiak, W.J., and Olejniczak, M. (2018). Precise Excision of the CAG Tract from the Huntingtin Gene by Cas9 Nickases. Front. Neurosci. *12*, 75.
25. Monteys, A.M., Ebanks, S.A., Keiser, M.S., and Davidson, B.L. (2017). CRISPR/Cas9 Editing of the Mutant Huntingtin Allele In Vitro and In Vivo. Mol. Ther. *25*, 12–23.
26. Ekman, F.K., Ojala, D.S., Adil, M.M., Lopez, P.A., Schaffer, D.V., and Gaj, T. (2019). CRISPR-Cas9-Mediated Genome Editing Increases Lifespan and Improves Motor Deficits in a Huntington's Disease Mouse Model. Mol. Ther. Nucleic Acids *17*, 829–839.
27. Cardinali, B., Provenzano, C., Izzo, M., Voellenkle, C., Battistini, J., Strimpakos, G., Golini, E., Mandillo, S., Scavizzi, F., Raspa, M., et al. (2022). Time-controlled and muscle-specific CRISPR/Cas9-mediated deletion of CTG-repeat expansion in the DMPK gene. Mol. Ther. Nucleic Acids *27*, 184–199.
28. Duvick, L., Southern, W.M., Benzow, K., Burch, Z.N., Handler, H.P., Mitchell, J.S., Kuivinen, H., Gadiparthi, U.K., Yang, P., Soles, A., et al. (2023). Delineating regional vulnerability in the neurodegenerative disease SCA1 using a conditional mutant ATXN1 mouse. Preprint at bioRxiv. https://doi.org/10.1101/2023.02.08.527710.
29. Platt, R.J., Chen, S., Zhou, Y., Yim, M.J., Swiech, L., Kempton, H.R., Dahlman, J.E., Parnas, O., Eisenhaure, T.M., Jovanovic, M., et al. (2014). CRISPR-Cas9 knockin mice for genome editing and cancer modeling. Cell *159*, 440–455.
30. Bosch, M.K., Nerbonne, J.M., and Ornitz, D.M. (2014). Dual transgene expression in murine cerebellar Purkinje neurons by viral transduction in vivo. PLoS One *9*, e104062.
31. Keiser, M.S., Boudreau, R.L., and Davidson, B.L. (2014). Broad therapeutic benefit after RNAi expression vector delivery to deep cerebellar nuclei: implications for spinocerebellar ataxia type 1 therapy. Mol. Ther. *22*, 588–595.
32. Chamberlin, N.L., Du, B., de Lacalle, S., and Saper, C.B. (1998). Recombinant adeno-associated virus vector: use for transgene expression and anterograde tract tracing in the CNS. Brain Res. *793*, 169–175.

33. Hakim, C.H., Kumar, S.R.P., Pérez-López, D.O., Wasala, N.B., Zhang, D., Yue, Y., Teixeira, J., Pan, X., Zhang, K., Million, E.D., et al. (2021). Cas9-specific immune responses compromise local and systemic AAV CRISPR therapy in multiple dystrophic canine models. Nat. Commun. *12*, 6769.

34. Dastidar, S., Ardui, S., Singh, K., Majumdar, D., Nair, N., Fu, Y., Reyon, D., Samara, E., Gerli, M.F.M., Klein, A.F., et al. (2018). Efficient CRISPR/Cas9-mediated editing of trinucleotide repeat expansion in myotonic dystrophy patient-derived iPS and myogenic cells. Nucleic Acids Res. *46*, 8275–8298.

35. Feng, G., Lu, J., and Gross, J. (2004). Generation of transgenic mice. Methods Mol. Med. *99*, 255–267.

36. Shultz, L.D., Ishikawa, F., and Greiner, D.L. (2007). Humanized mice in translational biomedical research. Nat. Rev. Immunol. *7*, 118–130.

37. Lykke-Andersen, S., and Jensen, T.H. (2015). Nonsense-mediated mRNA decay: an intricate machinery that shapes transcriptomes. Nat. Rev. Mol. Cell Biol. *16*, 665–677.

38. Buijsen, R.A.M., Hu, M., Sáez-González, M., Notopoulou, S., Mina, E., Koning, W., Gardiner, S.L., van der Graaf, L.M., Daoutsali, E., Pepers, B.A., et al. (2023). Spinocerebellar Ataxia Type 1 Characteristics in Patient-Derived Fibroblast and iPSC-Derived Neuronal Cultures. Mov. Disord. *38*, 1428–1442.

39. Borel, F., van Logtenstein, R., Koornneef, A., Maczuga, P., Ritsema, T., Petry, H., van Deventer, S.J., Jansen, P.L., and Konstantinova, P. (2011). In vivo knock-down of multidrug resistance transporters ABCC1 and ABCC2 by AAV-delivered shRNAs and by artificial miRNAs. J. RNAi Gene Silencing *7*, 434–442.

40. Grimm, D. (2011). The dose can make the poison: lessons learned from adverse in vivo toxicities caused by RNAi overexpression. Silence *2*, 8.

41. Snøve, O., Jr., and Rossi, J.J. (2006). Toxicity in mice expressing short hairpin RNAs gives new insight into RNAi. Genome Biol. *7*, 231.

42. Raemdonck, K., Vandenbroucke, R.E., Demeester, J., Sanders, N.N., and De Smedt, S.C. (2008). Maintaining the silence: reflections on long-term RNAi. Drug Discov. Today *13*, 917–931.

43. Chen, Y., Liu, X., Zhang, Y., Wang, H., Ying, H., Liu, M., Li, D., Lui, K.O., and Ding, Q. (2016). A Self-restricted CRISPR System to Reduce Off-target Effects. Mol. Ther. *24*, 1508–1510.

44. Yang, S., Li, S., and Li, X.J. (2018). Shortening the Half-Life of Cas9 Maintains Its Gene Editing Ability and Reduces Neuronal Toxicity. Cell Rep. *25*, 2653–2659.e3.

45. Keller, C.G., Shin, Y., Monteys, A.M., Renaud, N., Beibel, M., Teider, N., Peters, T., Faller, T., St-Cyr, S., Knehr, J., et al. (2022). An orally available, brain penetrant, small molecule lowers huntingtin levels by enhancing pseudoexon inclusion. Nat. Commun. *13*, 1150.

46. Monteys, A.M., Hundley, A.A., Ranum, P.T., Tecedor, L., Muehlmatt, A., Lim, E., Lukashev, D., Sivasankaran, R., and Davidson, B.L. (2021). Regulated control of gene therapies by drug-induced splicing. Nature *596*, 291–295.

47. Mizutani, A., Wang, L., Rajan, H., Vig, P.J.S., Alaynick, W.A., Thaler, J.P., and Tsai, C.C. (2005). Boat, an AXH domain protein, suppresses the cytotoxicity of mutant ataxin-1. EMBO J. *24*, 3339–3351.

48. Kawasaki, H., Kosugi, I., Sakao-Suzuki, M., Meguro, S., Tsutsui, Y., and Iwashita, T. (2016). Intracerebroventricular and Intravascular Injection of Viral Particles and Fluorescent Microbeads into the Neonatal Brain. J. Vis. Exp. *113*, 54164.

49. Robinson, J.T., Thorvaldsdóttir, H., Winckler, W., Guttman, M., Lander, E.S., Getz, G., and Mesirov, J.P. (2011). Integrative genomics viewer. Nat. Biotechnol. *29*, 24–26.

50. Rousseaux, M.W.C., Tschumperlin, T., Lu, H.C., Lackey, E.P., Bondar, V.V., Wan, Y.W., Tan, Q., Adamski, C.J., Friedrich, J., Twaroski, K., et al. (2018). ATXN1-CIC Complex Is the Primary Driver of Cerebellar Pathology in Spinocerebellar Ataxia Type 1 through a Gain-of-Function Mechanism. Neuron *97*, 1235–1243.e5.

51. Waxman, E.A., Dungan, L.V., DeFlitch, L.M., Merchant, J.P., Gagne, A.L., Goldberg, E.M., and French, D.L. (2023). Reproducible Differentiation of Human Pluripotent Stem Cells into Two-Dimensional Cortical Neuron Cultures with Checkpoints for Success. Curr. Protoc. *3*, e948.